

# The Cosmic Battery and the Inner Edge of the Accretion Disk

I. Contopoulos<sup>1\*</sup> and D. B. Papadopoulos<sup>2</sup>

<sup>1</sup>Research Center for Astronomy and Applied Mathematics, Academy of Athens, Athens 11527, Greece

<sup>2</sup>Department of Physics, Aristotle University of Thessaloniki, Thessaloniki 54124, Greece

Accepted . Received ; in original form

## ABSTRACT

The Poynting-Robertson Cosmic Battery proposes that the innermost part of the accretion disk around a black hole is threaded by a large scale dipolar magnetic field generated in situ, and that the return part of the field diffuses outward through the accretion disk. This is different from the scenario that the field originates at large distances and is carried inward by the accretion flow. In view of the importance of large scale magnetic fields in regulating the processes of accretion and outflows, we study the stability of the inner edge of a magnetized disk in general relativity when the distribution of the magnetic field is the one predicted by the Poynting-Robertson Cosmic Battery. We found that as the field grows, the inner edge of the disk gradually moves outward. In a fast spinning black hole with  $a \gtrsim 0.8M$  the inner edge moves back in towards the black hole horizon as the field grows beyond some threshold value. In all cases, the inner part of the disk undergoes a dramatic structural change as the field approaches equipartition.

**Key words:** accretion, accretion disks - X-ray binaries: black holes - magnetic fields

## 1 INTRODUCTION

Accretion of matter onto astrophysical black holes is a complex astrophysical process involving several physical sub-processes (general relativity, small and large scale magnetic fields, turbulence, plasma microphysics, etc.) Accretion proceeds in the form of a disk in which material moves slowly inward until it reaches an inner edge, beyond which it plunges in on dynamical timescales. Understanding where the accretion disk ends is of paramount importance in the two methods for measuring black hole spin, namely fitting the thermal X-ray continuum (Zhang, Cui & Chen 1997), and fitting the profile of the relativistically broadened iron  $K\alpha$  line (Fabian *et al.* 1989; see also McClintock *et al.* 2011 and references therein).

The inner edge of the disk is expected to be close to the radius of the Innermost Stable Circular Orbit (hereafter ISCO). It is well known that, for test particles, the position of the ISCO depends on the mass and angular momentum of the black hole. The situation is more complicated when, instead of test particles, one considers plasma in orbit around the black hole. It has been shown numerically that any turbulent magnetic field that may thread the plasma modifies its dynamics with respect to the idealized case of test particles, and the inner edge of the disk moves inward (Penna *et*

*al.* 2010). It has even been suggested that since the bulk of the disk is turbulent, there is no feature in the flow related to the ISCO, and the inner edge of the disk moves inward very close to the event horizon (Balbus 2012). What is still not very clear is what is the role of any large scale dipolar magnetic field present in the immediate vicinity of the central black hole. Igumenshchev (2008), Tchekhovskoy, Narayan & McKinney (2011) and others have shown numerically that a dipolar magnetic field advected inward from large distances can grow to equipartition, and can disrupt the process of accretion forming a ‘magnetically arrested disk’ (Narayan, Igumenshchev & Abramowicz 2003) interspersed with inward spiraling bundles of low-density plasma.

An independent line of thought, the Poynting-Robertson Cosmic Battery (hereafter PRCB; Contopoulos & Kazanas 1998; Kylafis, Contopoulos, Kazanas & Christodoulou 2011), proposes that the central dipolar magnetic field is generated in situ, with the return part of the field diffusing outward through the turbulent accretion disk. In other words, the origin of the large scale magnetic field is situated in the vicinity of the inner edge of the accretion disk, and not at large distances as in the latter case. In view of the importance of large scale magnetic fields in regulating the processes of accretion and outflows, we believe that there is still a lot to be learned from the theoretical study of axisymmetric accretion within the framework of the PRCB. We, therefore, decided to follow on the footsteps of Thorne

\* E-mail: icontop@academyofathens.gr (IC)

& Macdonald (1982) and Mobarrry & Lovelace (1986) and determine the inner edge of a magnetized disk in general relativity when the distribution of the large scale magnetic field is the one predicted by the PRCB. For simplicity, we ignore here the potentially important role of turbulent magnetic stresses (Balbus 2012). We begin in the next section with a presentation of our equations and physical simplifications of the problem. In § 3 we obtain our first results for a non-rotating (Schwarzschild) black hole, and in § 4 we extend our study in the most general case of a rotating (Kerr) black hole. Our conclusions are drawn in § 5.

## 2 THE RELATIVISTIC MHD EQUATIONS

Throughout this paper we adopt geometric units where  $G = c = 1$ . Semicolon stands for covariant derivative, comma for partial derivative. Latin indices denote spatial components (1–3), Greek indices denote space-time components (0–3), and ‘ $\sim$ ’ denotes the spatial part of vectors. In order to derive the relativistic MHD equations for our problem, we follow closely the 3+1 formulation of Thorne & Macdonald (1982) used by most researchers in the astrophysical community. We start with the most general 4-dimensional space-time geometry

$$ds^2 = g_{\mu\nu} dx^\mu dx^\nu, \quad (1)$$

and the Einstein field equations

$$R_{\mu\nu} - \frac{1}{2}g_{\mu\nu}R = 8\pi T_{\mu\nu} \quad (2)$$

with the Bianchi identities

$$(R^{\mu\nu} - \frac{1}{2}g^{\mu\nu}R)_{;\mu\nu} = 0, \quad (3)$$

where  $T^{\mu\nu}$ , the energy-momentum tensor, satisfies

$$T_{;\nu}^{\mu\nu} = 0. \quad (4)$$

We will restrict our analysis to space times where the torsion and expansion (but not the shear) vanish. In a cylindrical system of coordinates  $x^\mu \equiv (t, r, \theta, \phi)$  we henceforth also assume *steady-state*,  $(\dots)_{,t} = 0$ , and *axisymmetry*,  $(\dots)_{,\phi} = 0$ . The general 4-dimensional space-time geometry of Eq. (1) may be rewritten as

$$ds^2 = -\alpha^2 dt^2 + g_{\phi\phi}(d\phi - \omega dt)^2 + g_{rr}dr^2 + g_{\theta\theta}d\theta^2. \quad (5)$$

Notice that the theory of steady axisymmetric flows in ideal General Relativistic Magneto-Hydro-Dynamics (hereafter GRMHD) around a Schwarzschild black hole in (3+1) space-time split formulation was first developed by Mobarrry & Lovelace (1986). We choose fiducial ‘*zero-angular momentum observers*’ or ZAMOs who consider hypersurfaces  $t = \text{constant}$  as ‘slices of simultaneity’. ZAMOs move with 4-velocity

$$U^\mu = \frac{1}{\alpha}(1, 0, 0, \omega) \quad (6)$$

orthogonal to hypersurfaces of constant  $t$ . They are non-inertial observers with acceleration

$$a^\mu \equiv U_{;\nu}^\mu U^\nu. \quad (7)$$

Here, the lapse function of our observers  $\alpha \equiv (g_{t\phi}^2/g_{\phi\phi} - g_{tt})^{1/2}$ ,  $\omega \equiv -g_{t\phi}/g_{\phi\phi}$  and  $g_{ii}$  are in general functions of  $r$

and  $\theta$ . Finally, we define the tensor that projects 4-vectors onto hypersurfaces of constant  $t$  as

$$\gamma^{\mu\nu} \equiv g^{\mu\nu} + U^\mu U^\nu. \quad (8)$$

Our hydromagnetic system will be specified by the following choice for the energy-momentum tensor

$$T^{\mu\nu} = \rho u^\mu u^\nu + \frac{1}{4\pi}(F_\alpha^\mu F^{\nu\alpha} - \frac{1}{4}F_{\alpha\beta}F^{\alpha\beta}g^{\mu\nu}). \quad (9)$$

Here,  $u^\mu \equiv dx^\mu/d\tau$  is the fluid 4-velocity as measured by ZAMOs, and  $\rho$  is the density of the fluid. Notice that we have set here the pressure equal to zero, i.e. we have assumed a cold plasma.  $F^{\mu\nu}$  is the electromagnetic field tensor which is related to the electric and magnetic fields  $E^\mu, B^\mu$  measured by ZAMOs through

$$F^{\mu\nu} = U^\mu E^\nu - U^\nu E^\mu + \epsilon^{\mu\nu\lambda\rho} B_\lambda U_\rho. \quad (10)$$

Here,  $\epsilon_{\mu\nu\lambda\rho} \equiv \sqrt{|\det(g_{\mu\nu})|}[\mu\nu\lambda\rho]$  is the 4-dimensional Levi-Civita tensor. The GRMHD equations of motion are obtained from Eq.(4) supplemented by Maxwell’s equations of electrodynamics

$$F_{;\nu}^{\mu\nu} = 4\pi J^\mu, \quad F_{[\mu\nu;\alpha]} = 0, \quad (11)$$

where  $J^\mu$  is the electric current density that satisfies the charge conservation condition  $J_{;\mu}^\mu = 0$ . The electric current is related to the electric field through a generalized Ohm’s law. Eqs. (4) and (11) now read

$$\begin{aligned} \tilde{\nabla} \cdot \tilde{B} &= 0 \\ \frac{1}{\alpha} \tilde{\nabla} \cdot (\alpha \tilde{J}) &= 0 \\ D_\tau \tilde{B} &= 0 \\ D_\tau \tilde{\epsilon} + \frac{1}{\alpha^2} \tilde{\nabla} \cdot (\alpha^2 \tilde{S}) + W^{ij} \sigma_{ij} &= 0 \\ D_\tau \tilde{S} + \tilde{\sigma} \cdot \tilde{S} + \tilde{\epsilon} \tilde{a} + \frac{1}{\alpha} \tilde{\nabla} \cdot (\alpha \tilde{W}) &= 0, \end{aligned} \quad (12)$$

where,

$$\begin{aligned} \epsilon &= \Gamma^2 \rho + \frac{1}{8\pi}(\tilde{E}^2 + \tilde{B}^2), \quad \tilde{S} = \Gamma^2 \rho \tilde{v} + \frac{1}{4\pi} \tilde{E} \times \tilde{B}, \\ \tilde{W} &= \Gamma^2 \rho \tilde{v} \otimes \tilde{v} + \frac{1}{4\pi} \left[ -(\tilde{E} \otimes \tilde{E} + \tilde{B} \otimes \tilde{B}) + \frac{1}{2}(\tilde{E}^2 + \tilde{B}^2) \tilde{\gamma} \right], \\ \sigma^{ij} &= \frac{1}{2} \gamma^{i\mu} \gamma^{j\nu} (U_{\mu;\nu} + U_{\nu;\mu}), \quad \tilde{J} = \frac{\tilde{\nabla} \times (\alpha \tilde{B})}{4\pi\alpha}, \quad \text{and} \\ \Gamma &\equiv (1 - \tilde{v}^2)^{-1/2} \equiv (1 + \tilde{u}^2)^{1/2}. \end{aligned}$$

Here,  $\epsilon$  is the internal energy,  $\sigma^{\mu\nu}$  is the shear tensor of our system of reference,  $\tilde{v} \equiv \alpha^{-1} dx^i/dt$  is the fluid 3-velocity as measured by ZAMOs ( $\tilde{v} \equiv \Gamma^{-1} \tilde{u}$ ), and  $D_\tau$  is the Fermi derivative (see Appendix for details). We simplify the problem even further by assuming a dipolar magnetic field geometry, by restricting our analysis to the equatorial plane  $\theta = \pi/2$ , and by considering only the simplest case with no azimuthal magnetic torques. In  $(r, \theta, \phi)$  coordinates, symmetry dictates that

$$\begin{aligned} \tilde{v} &= (0, 0, v^\phi) \\ \tilde{B} &= (0, B^\theta, 0) \quad \text{with } B_{,\theta}^r \neq 0 \quad \text{in general,} \\ \tilde{E} &= (E^r, 0, 0) \quad \text{with } E_{,\theta}^r \neq 0 \quad \text{in general.} \end{aligned} \quad (13)$$

For several applications in astrophysics, perfect (infinite) conductivity is a valid approximation. In that limit, Ohm’s law yields the ideal MHD condition

$$u_\mu F^{\mu\nu} = 0 \quad (14)$$

which is equivalent to the statement that the electric field vanishes in a frame comoving with the fluid.

### 3 THE SCHWARZSCHILD METRIC

Before addressing the general case of an accreting spinning black hole, we will first consider the Schwarzschild metric on the equatorial plane where

$$\begin{aligned} ds^2 &= g_{tt}dt^2 + g_{rr}dr^2 + g_{\theta\theta}d\theta^2 + g_{\phi\phi}d\phi^2 \\ &= -\left(1 - \frac{2M}{r}\right)dt^2 + \left(1 - \frac{2M}{r}\right)^{-1}dr^2 \\ &\quad + r^2d\theta^2 + r^2d\phi^2. \end{aligned} \quad (15)$$

Here,  $M$  is the mass of the black hole. The lapse function is equal to  $\alpha = (1 - 2M/r)^{1/2}$ .  $\omega = 0$  and  $\sigma^{\mu\nu} = 0$ . Furthermore,

$$U^\mu = \frac{1}{\alpha} (1, 0, 0, 0), \quad (16)$$

$$a^i = \frac{M}{r^2} (1, 0, 0). \quad (17)$$

On the equatorial plane,  $B^r = E^\theta = 0$  due to symmetry, and according to Eqs. (10) & (14),

$$E^r = \alpha r^2 v^\phi B^\theta, \quad E^\theta = -\frac{1}{\alpha} v^\phi B^r, \quad (18)$$

with  $B_{,\theta}^r \neq 0$  and  $E_{,\theta}^\theta \neq 0$ . The  $r$ -component of the last one of Eqs. (12) now yields

$$\begin{aligned} &\left(1 - \frac{2M}{r}\right) \frac{(rv^\phi)^2}{r} - \frac{M}{r^2} \\ &- \frac{(rB^\theta)}{4\pi\rho r} \left\{ \alpha^2 [r(rB^\theta)_{,r} - B^r_{,\theta}] [1 - (rv^\phi)^2] \right. \\ &- \left. \frac{(rB^\theta)^2}{4\pi\rho r} \left\{ \frac{M}{r} - \alpha^2 (rv^\phi)^2 \left[ 1 + \frac{r(rv^\phi)_{,r}}{(rv^\phi)} \right] \right\} [1 - (rv^\phi)^2] \right\} \\ &= 0. \end{aligned} \quad (19)$$

Eq. (19) is the generalization of the Newtonian radial force-balance in Schwarzschild geometry. Given the distributions of  $\tilde{B}$  and  $\rho$  with  $r$  and  $\theta$  in the disk, it yields the distribution of the disk azimuthal angular velocity  $v^\phi$ . Those distributions can only be obtained through complex general relativistic magneto-hydrodynamic simulations. In this present work, however, we are only interested in determining the position of the innermost accretion disk layer where the PRCB is mostly active. We will thus address this problem analytically.

The vertical thickness  $h$  of the inner disk is a major uncertain parameter since it depends on several physical parameters (thermal pressure, radiation pressure from scattered photons, magnetic pressure), and is the subject of ongoing investigation. According to Fig. 1, we can approximate the value of the radial component of the magnetic field on the upper surface of the inner disk,  $B^r|_{+h}$ , with the value of the vertical component of the magnetic field on the disk midplane. Note that  $B^r = 0$  on the disk midplane. In other words,

$$B^r|_{+h} = -B^r|_{-h} \approx -rB^\theta \quad \text{and} \quad B^r_{,\theta} \approx \frac{r^2 B^\theta}{h} \equiv \lambda r B^\theta. \quad (20)$$

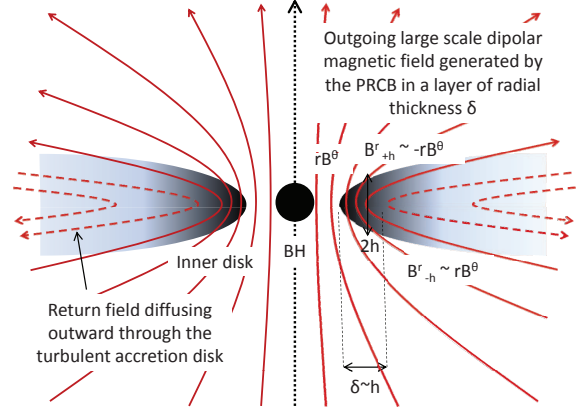


**Figure 1.** Sketch of innermost disk region where the large scale dipolar magnetic field is generated by the PRCB. Solid/dashed lines: outgoing/return field respectively. Dotted line:  $z$ -axis. The PRCB layer is the innermost disk region of radial extent  $\delta$ .

We have introduced here the parameter  $\lambda \equiv r/h$ . Furthermore, according to Contopoulos & Kazanas (1998), the dipole magnetic field originates in the innermost optically thin disk layer of radial extent  $\delta$  such that

$$\delta \sigma_T \frac{\rho}{m_p} \approx 1, \quad (21)$$

in which photons coming from the central accretion disk region penetrate. This is where the PR azimuthal electric current is generated. Beyond that layer, the magnetic field reverses polarity (see Fig. 1). Here  $\sigma_T$  is the Thomson cross section of photons scattered by the inner disk plasma orbiting electrons, and  $m_p$  is the proton mass. Contopoulos & Kazanas (1998) showed that, in order for the PRCB battery to operate secularly (i.e. continuously), thus generating a large scale dipolar magnetic field interior to the disk inner edge, the reverse polarity magnetic field needs to diffuse outward through the accreting plasma. This occurs naturally in a turbulent accretion disk with magnetic Prandtl number  $P_m \leq 1$ . We will here assume that

$$\delta \sim h, \quad (22)$$

although this may be generalized. Therefore, in the PR layer,

$$(rB^\theta)_{,r} \approx -\frac{rB^\theta}{h} \equiv -\lambda B^\theta. \quad (23)$$

Finally, in order to get rid of the radial derivative of  $v^\phi$ , we will assume a Keplerian velocity profile, namely

$$(rv^\phi)_{,r} \approx -\frac{v^\phi}{2}. \quad (24)$$

Under the above assumptions, eq. (19) becomes

$$\begin{aligned} &\left(1 - \frac{2M}{r}\right) \frac{(rv^\phi)^2}{r} - \frac{M}{r^2} \\ &+ \frac{v_A^2(r)}{r} \left\{ (2\lambda - 1) \left(1 - \frac{M}{r}\right) \right. \\ &- \left. (rv^\phi)^2 \left(2\lambda - \frac{3}{2} - \frac{2M}{r} \left(\lambda - \frac{3}{2}\right)\right) \right\} [1 - (rv^\phi)^2] \end{aligned}$$

$$= 0, \quad (25)$$

where,  $v_A^2(r) \equiv (rB^\theta)^2/4\pi\rho$ .

In order to determine the position of the disk inner edge, we will consider a virtual inward/outward displacement of the innermost layer of material of radial and vertical thickness  $\delta \approx h$  and  $h$  respectively, and study its stability. During that displacement, mass conservation implies that

$$2\pi r\delta h\rho = \text{constant}. \quad (26)$$

In order to proceed, we need to make certain further assumptions about how the various physical quantities in our problem vary during the above displacement. Our first assumption is that the angular momentum parallel to the symmetry axis per unit energy  $l$  is conserved, i.e. that

$$\alpha v^\phi \equiv \frac{d\phi}{dt} = l \frac{\alpha^2}{r^2}. \quad (27)$$

Our second assumption is that of flux freezing during the displacement. This implies that magnetic flux per unit mass is also conserved, i.e.

$$\frac{rB^\theta}{\rho h} = \text{constant}. \quad (28)$$

Our final assumption is that

$$\lambda \equiv \frac{r}{h} = \text{constant} \quad (29)$$

during the infinitesimal displacement. We see that under these assumptions,  $v_A^2$  varies inversely proportionally to  $r$  during the displacement away from the position of equilibrium, namely

$$v_A^2(r) \approx v_A^2 \frac{r_{\text{ISCO}}}{r}, \quad (30)$$

where  $v_A^2 \equiv v_A^2(r_{\text{ISCO}})$ .<sup>1</sup>

As we noted before, eq. (19) is the generalization of the Newtonian radial force-balance, which can also be seen as the zeroing of the first radial derivative of an effective potential  $V_{\text{eff}}$ . Therefore, in analogy to the Newtonian case, the displacement stability of the innermost disk layer is determined by the sign of the second radial derivative of  $V_{\text{eff}}$ . Marginal stability corresponds to zero second derivative of  $V_{\text{eff}}$ , i.e. to zero first derivative of eq. (19). When we substitute eqs. (27) & (30) in eq. (25), the condition for marginal stability, becomes

$$\mathcal{F}(x, \tilde{l}; \lambda, v_A^2 x_{\text{ISCO}}) = 0, \quad \text{and} \quad \frac{\partial}{\partial x} \mathcal{F}(x, \tilde{l}; \lambda, v_A^2 x_{\text{ISCO}}) = 0, \quad (31)$$

where,

$$\begin{aligned} \mathcal{F}(x, \tilde{l}; \lambda, v_A^2 x_{\text{ISCO}}) &\equiv \left(1 - \frac{2}{x}\right)^2 \frac{\tilde{l}^2}{x^3} - \frac{1}{x^2} \\ &+ \frac{v_A^2 x_{\text{ISCO}}}{x^2} \left\{ (2\lambda - 1) \left(1 - \frac{1}{x}\right) \right. \\ &\left. - \frac{\tilde{l}^2}{x^2} \left(1 - \frac{2}{x}\right) \left(2\lambda - \frac{3}{2} - \frac{2\lambda - 3}{x}\right) \right\} \left[ 1 - \frac{\tilde{l}^2}{x^2} \left(1 - \frac{2}{x}\right) \right], \quad (32) \end{aligned}$$

<sup>1</sup> Eq. (30) may be generalized as  $v_A^2(r) \approx v_A^2(r_{\text{ISCO}}/r)^\kappa$ .

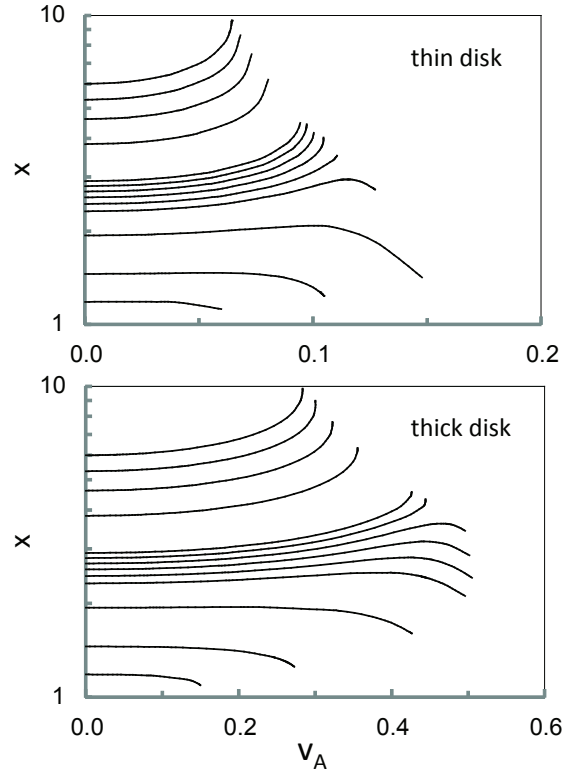


**Figure 2.** Dependence of  $x_{\text{ISCO}} \equiv r/M$  on the inner magnetic field strength for various black hole spin values  $a$ . At the points the curves end they begin to turn up and backwards. Top plot: thin disk ( $\lambda \equiv r/h = 10$ ). Bottom plot: thick disk ( $\lambda = 1$ ). The various curves from top to bottom correspond to  $\alpha = 0, 0.2, 0.4, 0.6, 0.8, 0.82, 0.84, 0.86, 0.88, 0.9, 0.95, 0.99, 0.999M$  respectively.

and  $x \equiv r/M$ ,  $\tilde{l} \equiv l/M$ . Notice that in this approach we do not need to derive an expression for  $V_{\text{eff}}(r)$ .

The position  $x_{\text{ISCO}}$  of the innermost marginally stable circular orbit as a function of our parameters  $\lambda$  and  $v_A^2$  is obtained numerically by eliminating  $\tilde{l}$  in the above system of equations (see Fig. 2 for  $a = 0$ ). For  $v_A \ll 1$ , the ISCO gradually moves outward from its unmagnetized position  $6M$ . In other words, *the magnetic field acts to destabilize the disk inner edge*, and the disk inner radius must be larger than  $6M$  for stability, in accordance with Lovelace *et al.* (1986). However, for higher values of  $v_A$  an ISCO ceases to exist. We conclude that, *in the presence of a large scale dipolar magnetic field, the ISCO moves outward, and eventually disappears as the field grows beyond a threshold value*. In the case of a thin disk ( $\lambda = 10$ ), that threshold value corresponds to  $v_A \sim 0.06$ . We will return to this important point in the Discussion section.

#### 4 THE KERR METRIC

The above can be directly generalized in the case of a spinning black hole. In Boyer-Lindquist coordinates, the Kerr metric reads:

$$ds^2 = g_{tt}dt^2 + 2g_{t\phi}dtd\phi + g_{t\theta}d\theta^2 + g_{\phi\phi}d\phi^2$$

$$\begin{aligned}
 &= -(1 - \frac{2Mr}{\Sigma})dt^2 - \frac{4Mar}{\Sigma}dtd\phi \\
 &\quad + \frac{\Sigma}{\Delta}dr^2 + \Sigma d\theta^2 + \frac{A}{\Sigma}d\phi^2
 \end{aligned} \tag{33}$$

where  $M$  is again the mass of the black hole,  $a$  its angular momentum per unit mass ( $0 \leq a \leq M$ ) and

$$\Delta \equiv r^2 - 2Mr + a^2, \quad \Sigma \equiv r^2 + a^2 \cos^2 \theta, \tag{34}$$

$$A \equiv (r^2 + a^2)^2 - a^2 \Delta. \tag{35}$$

The lapse function is equal to  $\alpha = (\Delta\Sigma/A)^{1/2}$ .  $\omega = 2aMr/A$ . On the equatorial plane ( $\theta = \pi/2$ ),

$$\alpha = \left(1 - \frac{2M}{r} + \frac{a^2}{r^2}\right)^{1/2} \frac{r^2}{\sqrt{A}}, \tag{36}$$

$$U^\mu = \frac{1}{\alpha} \left(1, 0, 0, \frac{2aMr}{A}\right), \tag{37}$$

$$a^i = \frac{Mr^2}{A} \left(1 + 2\frac{a^2}{r^2} - 4\frac{Ma^2}{r^3} + \frac{a^4}{r^4}, 0, 0\right). \tag{38}$$

As before,  $B^r = E^\theta = 0$  due to symmetry,

$$E^r = \frac{\Delta}{\alpha} v^\phi B^\theta, \quad E^\theta = -\frac{1}{\alpha} v^\phi B^r, \tag{39}$$

with  $B_{,\theta}^r \neq 0$  and  $E_{,\theta}^\theta \neq 0$ . In order to estimate the position of the ISCO when the PRCB is active, we will make the same simplifying assumptions as in the previous section. The  $r$ -component of the last one of eqs. (12) simplifies then considerably and becomes

$$\begin{aligned}
 &\Gamma_{\phi\phi}^r (v^\phi)^2 + \left[ \frac{1}{\alpha} (\Gamma_{t\phi}^r + \omega \Gamma_{\phi\phi}^r) + g_{\phi\phi} \sigma^{r\phi} \right] v^\phi + a^r \\
 &- \frac{v_A^2 r_{\text{ISCO}}}{r^2 \Gamma^4} \left\{ \frac{\Delta}{r^2} (\lambda + 1) + \lambda \right\} \\
 &- \frac{v_A^2 r_{\text{ISCO}}}{2r^3 \Gamma^2} \{X(v^\phi)^2 + Yv^\phi + Z\} = 0,
 \end{aligned} \tag{40}$$

where the detailed expressions for  $\sigma^{r\phi}$ ,  $X$ ,  $Y$ ,  $Z$ , the Christoffel symbols  $\Gamma_{t\phi}^r$ ,  $\Gamma_{\phi\phi}^r$  and the flow Lorentz factor  $\Gamma$  can be found in the Appendix. As before,  $v_A^2 \equiv v_A^2(r_{\text{ISCO}})$ .

The assumption that angular momentum parallel to the symmetry axis per unit energy  $l$  is conserved during a virtual infinitesimal displacement of the innermost layer of the disk is now generalized as

$$\begin{aligned}
 \alpha v^\phi &\equiv \frac{d\phi}{dt} - \omega \\
 &= \frac{-\Delta(a-l) + a(r^2 + a^2) - la^2}{-a(a-l)\Delta + (r^2 + a^2)^2 - la(r^2 + a^2)} - \omega \\
 &= l \frac{\left(1 - \frac{2M}{r}\right) \frac{r^2}{A} + \omega^2}{1 - \omega l}
 \end{aligned} \tag{41}$$

(Bardeen, Press & Teukolsky 1972; hereafter BPT72). When we substitute the above in eq. (40), we obtain a complicated expression of the form

$$\mathcal{G}(x, \tilde{l}; \lambda, v_A^2 x_{\text{ISCO}}) = 0, \tag{42}$$

and the condition for marginal stability becomes that

$$\frac{\partial}{\partial x} \mathcal{G}(x, \tilde{l}; \lambda, v_A^2 x_{\text{ISCO}}) = 0. \tag{43}$$

As before,  $x \equiv r/M$ , and  $\tilde{l} \equiv l/M$ . The position of the ISCO as a function of our two free parameters  $\lambda$  and  $v_A^2$  is obtained

as a solution of the above system of equations (42) & (43) for  $x$  and  $\tilde{l}$ . The solution for various values of the black hole spin parameter  $a$  is obtained numerically in Fig. 2 for two values of  $\lambda \equiv r/h$  that correspond to a thin and thick disk respectively. Similarly to the case of a Schwarzschild black hole, for small values of  $v_A$ , the ISCO always moves outward. However, for values of  $a \gtrsim 0.8M$ , an interesting transition takes place: as  $v_A$  grows beyond a threshold value, *the ISCO moves back inward*. As we will now see, this result complicates the observational determination of the black hole spin.

## 5 DISCUSSION

The displacement of the ISCO in the presence of a large scale magnetic field generated in situ has direct implications in the currently most promising method for measuring black hole spin, namely fitting the thermal X-ray continuum (Zhang et al. 1997). This method requires knowledge of both the Schwarzschild radius and the radius of the inner edge of the disk, i.e. it requires knowledge of  $x_{\text{ISCO}}$ . As is shown in BPT72, in an unmagnetized disk,  $x_{\text{ISCO}}$  is one-to-one related to the spin of the black hole. In the present work, we showed that  $x_{\text{ISCO}}$  depends also on the value of the magnetic field accumulated in the innermost region of the accretion disk. This result introduces one extra complication.

In particular, the disappearance of the ISCO as the field grows towards equipartition (defined in this context as  $v_A \rightarrow 1$ ) is an indication for a dramatic change in the structure of the accretion disk in the presence of a strong enough magnetic field generated by the PRCB. It is natural to speculate that, when the conditions for marginal stability of the inner edge cannot be satisfied, the accumulated magnetic field will escape outward through magnetic Rayleigh-Taylor-type instabilities, as proposed in Igumenshchev (2008), Tchekhovskoy, Narayan & McKinney (2011), and Kylafis *et al.* (2012). As a result, the accumulated magnetic field will decrease, the ISCO will reappear close to its unmagnetized disk position, and the disk will undergo a new phase of field growth and evolution. For a stellar mass black hole, the time required for equipartition field growth is on the order of a few hours to a few days (Contopoulos & Kazanas 1998; Kylafis *et al.* 2012), whereas the intervals of dramatic disk structure change are expected to be much shorter (dynamic timescales).

For black holes with spin parameter  $a < 0.8M$ , the inner edge of the disk is expected to be outside its unmagnetized position, therefore the thermal X-ray continuum fitting method will on average yield a *systematically smaller* value for the black hole spin. On the other hand, for fast spinning black holes with  $a \gtrsim 0.8M$ , the inner edge of the disk moves to lower values, and in those cases the thermal X-ray continuum fitting method will on average yield *systematically larger* values for the black hole spin. This result introduces an *artificial segregation* in our observational method that may be related to the seeming absence of evidence for the black hole spin powering the jets in X-ray binaries (Fender, Gallo & Russell 2010; see however also Narayan & McClintock 2012). In other words, the introduction of one extra free parameter, namely the amount of magnetic flux accumulated around the inner edge of the disk, complicates

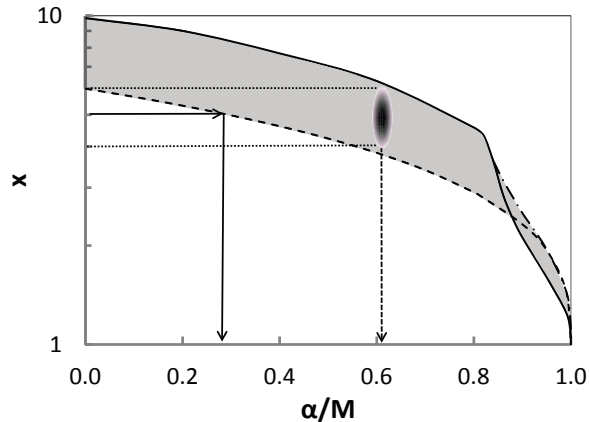


**Figure 3.** Range of  $x_{\text{ISCO}}$  values as a function of the black hole spin parameter  $a$  for a thick disk  $r/h = 1$ . Dashed curve: unmagnetized disk. Solid curve: maximally magnetized inner disk that supports an ISCO. Shaded region: range of  $x_{\text{ISCO}}$  values when  $0 \leq v_A \leq v_A|_{\text{max}}$ . Diffuse cloud: range of  $x_{\text{ISCO}}$  values obtained for the X-ray black hole binary LMC X-3 over a period of 25 years. Left vertical arrow: average spin parameter of unmagnetized disk. Right vertical arrow: spin parameter that yields the observed range of  $x_{\text{ISCO}}$  values in the context of the PRCB.

the direct determination of the black hole spin through the knowledge of  $x_{\text{ISCO}}$  alone.

The above are summarized in Fig. 3 where we show the range of  $x_{\text{ISCO}}$  values as a function of  $a$  for a thick disk ( $r/h = 1$  at its inner edge). The dashed curve corresponds to the unmagnetized disk (BPT72), whereas the solid curve to a maximally magnetized disk that supports an ISCO. The dashed-dotted curve corresponds to the maximum values of  $x_{\text{ISCO}}$  reached as the inner field ( $v_A$ ) grows in a spinning black hole with  $a \gtrsim 0.8M$ . In other words, according to our simplified model of the inner disk, observations of  $x_{\text{ISCO}}$  must lie in the shaded region. As an example, in the most studied object, LMC X-3, estimates of  $x_{\text{ISCO}}$  range from about 4 to about 6 (Steiner *et al.* 2010, assuming a canonical value for the black hole mass equal to  $7.5M_{\odot}$ ). If the PRCB did not operate and the disk were unmagnetized, these values would yield an average black hole spin value  $a \sim 0.3M$  (McClintock *et al.* 2011). It is natural, though, to expect that the PRCB does operate as described above, and that the various estimates of  $x_{\text{ISCO}}$  simply correspond to the various stages of magnetic field growth that the source is found to be in. As shown in Fig. 3, in this context, a more natural value of the black hole spin in LMC X-3 would then be  $a \sim 0.6M$ .

Finally, the reader may wonder in what respect the PRCB manifests itself in the inner disks structure differently from flux advection from large distances. One way to differentiate between the two is the radial width  $\delta$  of the PRCB layer over which  $B^{\theta}$  changes significantly. In the PRCB and a thin disk, our parameter  $r/\delta \sim \lambda$  is expected to be on the order of 10. On the other hand, in the PRCB and a thick disk, as well as in a disk where the magnetic field is advected inward from large distance,  $\lambda$  is expected to be on

the order of unity. Another way to differentiate between the two possibilities has to do with the particular cyclic disk variability central to the PRCB, namely intervals of secular field growth (hours, days) separated by intervals of strong (msec) disk variability. Our present investigation on the role of the PRCB in determining the structure of the inner disk is certainly not exhaustive and will continue in the framework of Program ARISTEIA of the General Secretariat for Research and Technology of Greece.

## ACKNOWLEDGMENTS

We thank Drs. Dimitris Christodoulou and Demos Kazanas for their comments and suggestions. D.B.P. would like to thank the Institute für Astronomie und Astrophysik Abteilung Theoretische Astrophysik of Eberhard Karls Universität Tübingen where part of this work was performed.

## REFERENCES

- Balbus, S. A. 2012, MNRAS, L443  
 Bardeen, J. M., Press, W. H. & Teukolsky, S. A. 1972, ApJ, **178**, 347 (BPT72)  
 Contopoulos, I. & Kazanas, D. 1998, ApJ, **508**, 859  
 Contopoulos, I., Kazanas, D., Christodoulou, D. M. & Gabuzda, D. C. 2009, ApJ, **702**, 148  
 Fabian, A. C., Rees, M. J., Stella, L. & White, N. E. 1989, MNRAS, **238**, 729  
 Fender, R. P., Gallo, E. & Russell, D. 2010, MNRAS, **406**, 1425  
 Igumenshchev, I. V. 2008, ApJ, **677**, 317  
 Kylafis, N. D., Contopoulos, I., Kazanas, D. & Christodoulou, D. M. 2012, A&A, **538**, 5  
 Lovelace, R. V. E., Mehanian, C., Mobarry, C. M. & Sulkanen, M. E. 1986, ApJS, **62**, 1  
 Macdonald, D. & Thorne, K., S. 1982, MNRAS, **198**, 345  
 McClintock, J. E. *et al.* 2011, Class. & Quantum Grav., **28**, 114009  
 Mobarry, C. M. & Lovelace, R. V. E. 1986, ApJ, **309**, 455  
 Narayan, R. & McClintock, J. E. 2012, MNRAS, **419**, 69  
 Narayan, R., Igumenshchev, I. V. & Abramowicz, M. A. 2003, PASJ, **55**, 69  
 Penna, R. F. *et al.* 2010, MNRAS, **408**, 752  
 Steiner, J. F. *et al.* 2010, ApJ, **718**, 117  
 Tchekhovskoy, A., Narayan, R. & McKinnery, J. C. 2011, MNRAS, **418**, 79  
 Thorne, K. S. & Macdonald, D. 1982, MNRAS, **198**, 339  
 Zhang, S. N., Cui, W. & Chen, W. 1997, ApJ, **482**, L155

## APPENDIX A:

Various expressions used throughout the paper are defined below according to Thorne & Macdonald (1982):

$$\tilde{\nabla} \cdot \tilde{A} \equiv A_{;j}^j, \quad (\tilde{\nabla} \times \tilde{A})^i \equiv \epsilon^{ijk} A_{k;j}$$

$$D_{\tau} A^{\beta} \equiv A_{;\mu}^{\beta} U^{\mu} - U^{\beta} U_{\mu;\nu} A^{\mu} U^{\nu}$$

$$\tilde{A} \cdot \tilde{B} \equiv A^i B_i, \quad (\tilde{A} \times \tilde{B})^i \equiv \epsilon^{ijk} A_j B_k, \quad (\tilde{A} \otimes \tilde{B})^{ij} \equiv A^i B^j$$

Here,  $\epsilon^{ijk} \equiv [ijk]/\sqrt{|\det(\gamma_{ij})|}$  is the spatial Levi-Civita tensor. On the equatorial plane ( $\theta = \pi/2$ ),

$$\Delta = r^2 - 2Mr + a^2, \quad \Sigma = r^2, \quad A = r^4 + a^2 r^2 + 2Ma^2 r$$

$$\Gamma = \left[ 1 - \frac{A}{r^4} (rv^\phi)^2 \right]^{-1/2}$$

$$\Gamma_{t\phi}^r = -\frac{Ma\Delta}{r^4}, \quad \Gamma_{rr}^r = -\frac{Mr - a^2}{\Delta r}$$

$$\Gamma_{\theta\theta}^r = -\frac{\Delta}{r}, \quad \Gamma_{\phi\phi}^r = -\frac{\Delta}{r} \left[ 1 - \frac{Ma^2}{r^3} \right]$$

$$\begin{aligned} \Gamma_{k1}^k &\equiv \Gamma_{rr}^r + \Gamma_{\theta r}^\theta + \Gamma_{\phi r}^\phi \\ &= \frac{r}{\Delta} \left( 2 - \frac{5M}{r} + \frac{2a^2}{r^2} - \frac{Ma^2}{r^3} \right) \end{aligned}$$

$$\sigma^{r\phi} = \sigma^{\phi r} = -\frac{Ma\Delta(a^2 + 3r^2)}{rA\sqrt{A\Delta}}$$

$$a^r = \frac{Mr^2}{A} \left( 1 + 2\frac{a^2}{r^2} - 4\frac{Ma^2}{r^3} + \frac{a^4}{r^4} \right)$$

$$\omega = \frac{2Mar}{A}, \quad \alpha = \sqrt{\frac{\Delta r^2}{A}}$$

$$\begin{aligned} X &\equiv \left( \frac{\Delta}{\alpha} \right)^2 \left\{ -\frac{a^r r^2}{\Delta} + Q - \frac{1}{\Delta} \Gamma_{\theta\theta}^r - \frac{1}{\Delta} \Gamma_{\phi\phi}^r (\gamma^{\phi\phi} r^2) \right\} \\ &\quad + 2 \left( \frac{\Delta}{\alpha} \right) \left( \frac{\Delta}{\alpha} \right)_{,r} + 2 \frac{v_{,r}^\phi}{v^\phi} \frac{\Delta^2}{\alpha^2} \end{aligned}$$

$$Y \equiv -2 \frac{r^2}{\alpha} (\Gamma_{t\phi}^r + \omega \Gamma_{\phi\phi}^r)$$

$$Z \equiv -a^r r^2 - \Delta Q - \Delta_{,r} + \Gamma_{\theta\theta}^r - \Gamma_{\phi\phi}^r (\gamma^{\phi\phi} r^2)$$

$$Q = \frac{\alpha_{,r}}{\alpha} + 2\Gamma_{rr}^r + \Gamma_{\theta r}^\theta + \Gamma_{\phi r}^\phi$$